Trodden DG, Haroutunian M.

Effects of Ship Manoeuvring Motion on NO_X Formation.

***Ocean Engineering* 2018, 150, 234–242.**

Effects of Ship Manœuvring Motion on NO_X Formation

D.G. Trodden[a,*], M. Haroutunian[a]

[a]*School of Marine Science and Technology, Armstrong Building, Newcastle University, Newcastle upon Tyne, NE1 7RU, United Kingdom.*

Abstract

Oxides of Nitrogen (NO_X) are harmful to human health, as such their emissions are monitored and controls are becoming increasingly stringent.

NO_X formation is dependent on engine running conditions and therefore on ship operation; there will be differences in the amount of NO_X produced when a ship is travelling in a straight line, compared to when manœuvring.

Ships tend to spend more time in manoeuvring conditions around population dense areas such as inland waterways, compared to when on the deep sea. It is therefore important to investigate the difference that manœuvring motion has on NO_X production, compared to steady-state running.

Emission factors, which are often given as a function of fuel oil consumption and based upon steady-state conditions, are frequently used to estimate engine emissions. In this paper, an emission factor is developed using a numerical engine model coupled with chemical kinetics computations. The same model, coupled to a ship manœuvring simulator is then used to compare NO_X formation during manœuvring operations.

It is demonstrated that during manœuvres, the developed simulator exhibits significant differences in NO_X formation, compared to the commonly used emission factor approaches.

Keywords: Simulation, Manoeuvring, Emissions, Transient Operation, Inland Waterways

Nomenclature

β_P Drift angle at propeller plane $[rad]$

δ_R Rudder angle $[rad]$

ρ Density $[kgm^{-3}]$

ϕ Crank shaft anlge $[rad]$

a_H Coefficient to account for interaction between the hull and rudder $[-]$

B Ship's beam $[m]$

BAR Propeller's Blade Area Ratio [-]

CO_2 Carbon Dioxide

CH_4 Methane

D Propeller diameter $[m]$

F_N Force normal to the rudder from deflection of incident flow $[N]$

I_{zz} Mass moment of inertia about the Z axis $[Kgm^2]$

J_{zz} Yaw added mass moment of inertia $[Kgm^2]$

K_Q Propeller torque coefficient [-]

K_T Propeller thrust coefficient [-]

L_{oa} Ship length overall $[m]$

LNG Liquefied Natural Gas

m Mass $[kg]$

m_x Surge added mass $[Kg]$

m_y Sway added mass $[Kg]$

N_H Moment around midship (yaw) due to the ship hull's interaction with the water $[Nm]$

N_{H_0} Yaw moment without added mass terms $[Nm]$

N_R Moment around midship (yaw) due to the action of the rudder $[Nm]$

N_P Moment around midship (yaw) due to action of the propeller $[Nm]$

n Propeller's rotational speed $[revolutions\ s^{-1}]$

n_c Crankshaft rotational speed $[revolutions\ s^{-1}]$

NO_X Reference to Nitrogen Oxides generally

NO_2 Nitrogen Dioxide

N_2O Nitrous Oxide

NO Nitric Oxide

*Corresponding author

Email addresses: david.trodden@ncl.ac.uk (D.G. Trodden), maryam.haroutunian@ncl.ac.uk (M. Haroutunian)

P Propeller pitch $[m]$, or Pressure $[Nm^{-2}]$, depending on context

r Yaw rate $[\text{rad}s^{-1}]$

r_c Crank radius $[m]$

T Ship's draught $[m]$, or Temperature $[K]$, depending on context

T_{inside} Instantaneous temperature inside cylinder $[K]$

T_{outside} Instantaneous temperature outside cylinder $[K]$

t Time $[s]$

t_R Rudder drag correction coefficient $[-]$

tdf Thrust deduction factor [-]

U Heat transfer coefficient for conduction/convection $[Wm^{-2}]$

u Surge velocity $[ms^{-1}]$

UKC Under Keel Clearance, usually given as % of draught $[ms^{-1}]$

V_v Resultant ship velocity $[ms^{-1}]$

v Sway velocity $[ms^{-1}]$

v_o Sway velocity at midship $[ms^{-1}]$

w_P Wake fraction at propeller plane [-]

X_H Force in the X (surge) direction due to the ship hull's interaction with the water $[N]$

X_{H_0} Ship resistance in calm water $[N]$

X_R Force in the X (surge) direction due to the action of the rudder $[N]$

X_P Force in the X (surge) direction due to action of the propeller $[N]$

x_H X coordinate of the point of application of the lift from the hull with respect to amidships $[m]$

x_P X coordinate of propeller with respect to midships $[m]$

x_R X coordinate of the centre of pressure of the rudder with respect to midships $[m]$

Y_H Force in the Y (sway) direction due to the ship hull's interaction with the water $[N]$

Y_{H_0} Sway force without added mass terms $[N]$

Y_R Force in the Y (sway) direction due to the action of the rudder $[N]$

Y_P Force in the Y (sway) direction due to action of the propeller $[N]$

1. Introduction

Mandatory regulations from bodies such as the International Maritime Organisation (IMO) restrict the amount of exhaust gas emissions produced by ships (IMO, 2005).

In order to meet these requirements of increasingly stringent regulations, the maritime sector is turning to alternative fuels such as Liquefied Natural Gas (LNG). LNG has shown to be a viable alternative to conventional Diesel fuel, in terms of both emissions and cost (Burel et al., 2013). Projects such as the LNG Masterplan (Seitz et al., 2015) demonstrate LNGs viability, especially for inland waterways where the LNG infrastructure for refuelling can be established with relative ease. Hence LNG is chosen as the main propulsion fuel used in this study.

Certain exhaust gas species are known to be harmful to human health (Kampa and Castanas, 2008), and contribute to environmental problems such as global warming and acid rain. For these reasons mechanisms are required to estimate the amount of exhaust gas emissions produced from operating ships.

The focus of this paper is around NO_X formation from transient propulsion loading, not only because of its associated impact on human health and the environment, but for the reason that other salient species such as Carbon Dioxide (CO_2) or Oxides of Sulphur (SO_X) can be adequately estimated using *emission factors* based upon stoichiometric combustion, as will be shown in this study.

There are mechanisms currently capable of estimating the amount of NO_X produced by combustion. Perhaps the most simple are those based upon emission factors. These can either be based upon a direct relation to fuel consumption (MEPC, 2014), or as a function of engine power and speed (Murphy and Pazouki, 2012). These methods give a rough estimate and are relevant to specific fuel and engine types. Emission factor based approaches provide an extremely computationally fast estimate of emissions.

Zeldovich (1946) provides a mechanism to estimate the thermal NO formation. Methods based upon these approaches have a limited number of reactions and it can be challenging to estimate required oxygen atom concentration. Zeldovich based mechanisms are however relatively computationally fast.

Chemical kinetics analysis can accurately model NO_X formation, as well as many other species, and with increased modern computing power, a chemical kinetics routine can be comfortably incorporated into a numerical engine model to provide estimates of emissions

under varying loading conditions.

The use of chemical kinetics solvers allows analysis of how different conditions can influence the speed of reactions and yield details about the reaction's mechanism and transition states. The reaction mechanism is a step by step sequence of elementary reactions by which overall chemical change occurs. The use of a chemical kinetics solver therefore suites itself well to the study of unsteady behaviour on emissions.

A number of existing chemical kinetics solvers exist, including ChemKin (Reaction Design, 2017), Cantera (Goodwin et al., 2017) and the Kinetic PreProcessor (Damian et al., 2017). In this study, Cantera was chosen due to its performance, robustness and ease of portability into existing ship manœuvring simulator code.

There are currently several different perspectives on numerically modelling engines, depending upon the intended application. Hountalas (2000) found that due to engine specification and diversity, a specific software needs to be written for each application. Murphy et al. (2015) have developed a time-domain based engine simulator, considering differing gas properties under full, part or transient loading. For particularly detailed engine models, accounting for elements such as cylinder shapes or injection spray patterns, Computational Fluid Dynamic methods may be employed (Kilpinen, 2010). These latter models require significant amounts of computing resources and engine detail, which are impracticable for certain applications such as initial design or emission surveys for a stretch of water, which this study aims to address.

Among the most popular techniques used to model engine performance are the quasi-steady flow models, and the filling and emptying models. Quasi-steady models predict performance characteristics from a thermodynamics based analysis, calculating mass flow rates into and out of the cylinder through inlet and exhaust valves. If the pressure variation with respect to time is small, then such methods can be useful. In the filling-and-emptying models, manifolds are represented as finite volumes, where the mass of gas can vary with time. In transient conditions, where engine load varies with time, manifold conditions will vary. It is this latter method which is utilised in this study.

Soares et al. (2015) uses an engine model in conjunction with a chemical kinetics routine to estimate exhaust emissions from a two-stroke Diesel engine. The results of which are validated against data from real engines.

In order to obtain realistic, service condition loading scenarios on a numerical engine model, the current study uses a ship manœuvring simulator coupled to the engine model. This provides the engine model with dynamic loading experienced by the propeller as the ship manœuvres and thus the basis to estimate exhaust gas emissions over a route.

Numerous ship manœuvring simulators exist, including ones which specialise in inland waterway applications and can account for phenomena such as shallow water effects (Eloot and Vantorre, 2003). They are usually based in the time domain, which make them well suited for estimation of NO_X formation, where residence time is a critical factor.

Ship manœuvring simulators are also coupled with engine simulators and are commonly found in Full Mission Bridge Simulators (Kongsberg Gruppen, 2017). These latter simulators are for the purposes of training crew and used to provide feedback between the engine and deck departments of a ship.

Currently the effect of a ship's manœuvring motion is not taken into account when calculating the production of emissions. This paper aims to address this and its significance by investigating the effects of manœuvring motion on NO_X formation from a propulsion system fuelled by LNG, although the methodology is applicable to other fuels and exhaust gas species.

Whilst applicable to ocean going vessels, this study concentrates on inland waterway transport, such as found on the Rhine-Main-Danube Canal. This waterway stretches from the Black Sea to the North Sea and navigable throughout its length by large barges. The canal passes through many towns and cities where the effects of NO_X emissions, being toxic to humans, are of interest. The waterway has numerous bends which demand the propulsion system to operate away from the steady-state design point whilst navigating these passages. This deviation from steady-state running conditions, either due to environmental loading or manœuvring, has strong implications for estimation of NO_X emissions. The transient operation can produce fuel consumption and exhaust gas emission estimates that are significantly different to averaged steady-state calculations, commonly used to estimate emissions.

Significant challenges arise when obtaining an accurate numerical manœuvring simulation model in confined waters. Full scale ship manœuvring trials in shallow water are rare. The ship's kinematics, forward speed, rate of turn, drift angle, response of propulsion, and the control system are all affected by operation in restricted water. The most accurate way of modelling ship manœuvring behaviour, especially in shallow water, is from the use of model tests (Vantorre, 2003). The aim of this study is to obtain an initial estimate of how the magnitude of emissions changes with the unsteady state experienced when a ship is manœuvring. Thus at

this stage, rather than carry out costly and time consuming model tests, this research utilises established corrections for several confined water effects. A detailed overview of methods can be found in the report of ITTC Manoeuvring Committee (2002). Although the effects of muddy bottoms on ship manœuvrability are being developed (Delefortrie et al., 2005), the effect has been excluded from this initial investigation.

Once a realistic relationship between emissions and unsteady manœuvring behaviour is shown to be of significance, then numerical models can be further refined and tuned for accuracy on particular ships and propulsion units.

Simulation of a ship's manoeuvring motion has been examined by various people, including the whole-ship type approach of Abkowitz (1964), and the modular approach used by Hirano (1981) and Oltmann and Sharma (1984). An advantage of the modular approach is being able to study separate components (such as rudder geometry) of the ship without requiring to arrive at new manœuvring derivatives. It is this approach that is used in this study. These techniques solve a series of Ordinary Differential Equations (ODEs) in the time domain, which is especially suited when it comes to coupling with an engine simulator, whose emission estimates are dependent on time.

2. Methodology

In order to simulate the effects of transient manœuvring motion on NO_X formation, a NO_X emission factor is formulated by running the developed simulator in the calm-water, dead-ahead condition at the basis vessel's design speed. The resulting emission factor is a function of fuel consumption. This emission factor is then used to estimate NO_X emissions throughout the time history of the vessel's manœuvre at the associated engine loading. Unsteady NO_X emissions are also calculated by coupling the ship manœuvring and engine simulator to a chemical kinetics solver. These resulting emissions account for unsteady manœuvring behaviour, and the unsteady response of the engine. The results from the steady-state emission factor estimates are then compared to the values obtained from the chemical kinetics calculations.

The time resolution required for a ship manœuvring simulation is far lower than that required to model NO_X formation from the engine model, approximately by a factor of 10^5. To ensure fast computation times, two time resolutions are used; one for manœuvring, another for engine simulation. The engine model is called at each time step of the manœuvring model and run for the duration of the engine model's time step. This assumes that the engine loading will not change significantly over the time step of the manœuvring model, which is chosen to reflect this.

2.1. Basis Vessel

The basis vessel used in this analysis is a single screw inland waterway barge, the main particulars of which have been chosen for passage through the Rhine-Main-Danube Canal, and can be found in Table 1. The vessel is powered by a four-stroke LNG fuelled Diesel cycle engine.

Table 1: Main Particulars of Basis Vessel.

Ship	Propeller
$L_{oa} = 110\ m$	$D = 1.90\ m$
$B = 11.3\ m$	$P = 1.47\ m$
$T = 3.4\ m$	$BAR = 0.594$
$V_S = 14.8\ km/h$	

2.2. Basis Manœuvres

The manœuvres performed by the basis vessel are part of a standard 35° rudder turning circle, and a 20/20 zig-zag manœuvre. This ensures repeatability of the analysis. Whilst the turning circle manœuvre is quite severe, it is not unrealistic for a ship to undergo a $\sim 180°$ heading change on sections of the Rhine-Main-Danube Canal, for example near the town of Hinova on the Romanian/Serbian boarder. This turning circle manœuvre will also move the operation point further away from the design point when compared to the zig-zag manœuvre. The zig-zag manœuvre is intended to mimic manœuvres more commonly experienced on inland waterways.

The 35° rudder turning circle manœuvre is represented in Figure 1, and the 20/20 zig-zag manœuvre is represented in Figure 3. The simulation for manœuvres was truncated after 350 seconds. Taking into account the induced sway and yaw motions, as well as the dynamic response of the propulsion system, the resulting change in ship speed can be seen in Figure 2 for the turning circle and Figure 4 for the 20/20 zig-zag manœuvre, and shows some effects associated with the confined waters of the canal.

2.3. Manœuvring Simulation

A three degree-of-freedom manœuvring simulator has been developed in the manoeuvring motions of surge, sway and yaw, and relates the dynamic loading

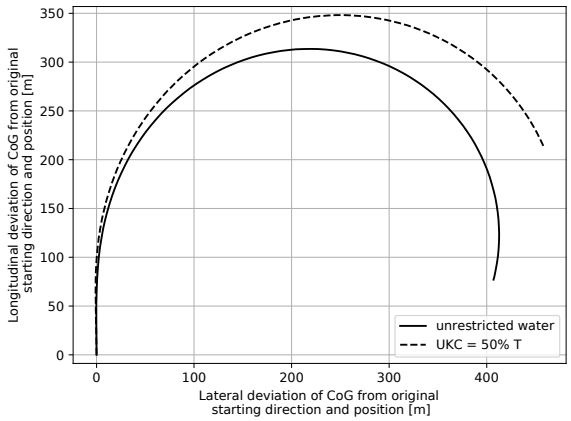

Figure 1: Ship track during turning circle in unrestricted water and with an Under Keel Clearance of 50% Draught.

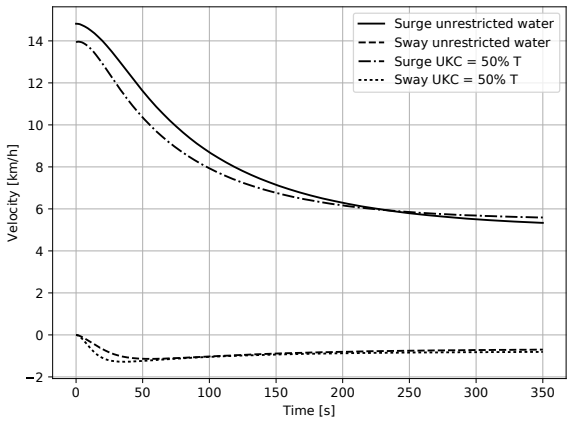

Figure 2: Surge and sway velocities during turning circle manœuvre in unrestricted water and with an Under Keel Clearance of 50% Draught.

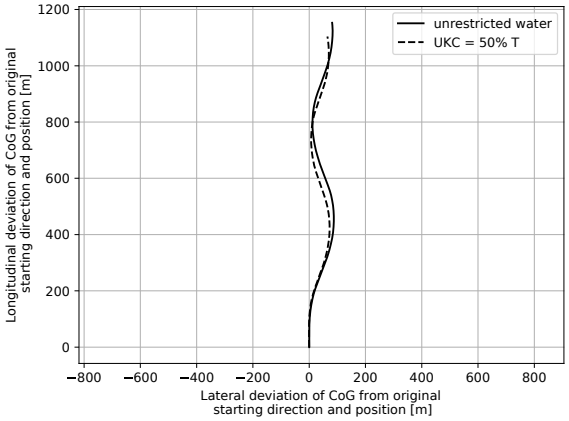

Figure 3: Ship track during zig-zag manœuvre in unrestricted water and with an Under Keel Clearance of 50% Draught.

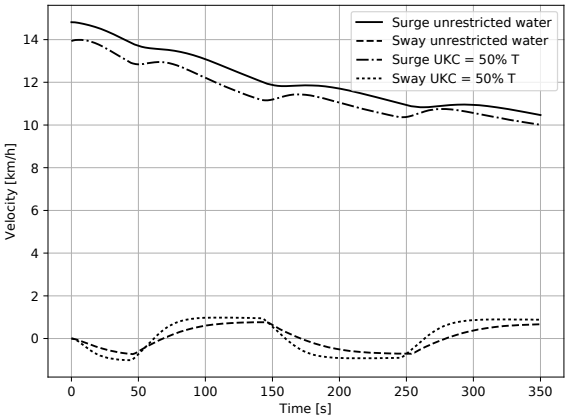

Figure 4: Surge and sway velocities during zig-zag manœuvre in unrestricted water and with an Under Keel Clearance of 50% Draught.

on the propeller to the engine model (Trodden et al., 2016).

The approach taken in the development of the simulator used in this study is to solve a series of differential equations in the time domain, described in the following subsections.

2.3.1. Equations of Motion

It can be shown that the equations of motion in surge, sway and yaw, with the origin located at the centre of gravity, can be written as equation 1.

$$m(\dot{u} - rv) = X_H + X_R + X_P \qquad \text{Surge} \qquad (1a)$$

$$m(\dot{v} + ru) = Y_H + Y_R + Y_P \qquad \text{Sway} \qquad (1b)$$

$$I_{zz}\dot{r} = N_H + N_R + N_P \qquad \text{Yaw} \qquad (1c)$$

Where m is the mass of the ship, I_{zz} is the mass moment of inertia around a vertical axis. u and v is the ship's velocity in pure surge and sway respectively, and r is the ship's rate of change of heading. The subscripts H, R, P in equation 1, denote hull, rudder and propeller respectively. The methodologies used to estimate these contributions are briefly discussed next.

2.3.2. Hull

The longitudinal force on the ship's hull, X_H, transverse force on the ship's hull, Y_H, and the yaw moment on the ship's hull, N_H can be written as equations 2.

$$X_H = -m_x\dot{u} + \left(m_y + X_{vr}\right)v_o r + X_{H_o}(u) \qquad (2a)$$

$$Y_H = -m_y\dot{v} - m_x ur + Y_{H_o}(v_o, r) \qquad (2b)$$

$$N_H = -J_{zz}\dot{r} + N_{H_o}(v_o, r) \qquad (2c)$$

The hull's manœuvring derivatives are obtained from the study of Inoue et al. (1981).

2.3.3. Rudder

The calculation for the longitudinal force (drag) X_R, transverse force, Y_R and turning/yawing moment N_R imposed upon the ship by the action of the rudder are expressed in the form of equations 3.

$$X_R = -(1 - t_R) F_N \sin \delta_R \tag{3a}$$

$$Y_R = -(1 - a_H) F_N \cos \delta_R \tag{3b}$$

$$N_R = -(x_R + a_H x_H) F_N \cos \delta_R \tag{3c}$$

Where, F_N is the force normal to the rudder, t_R is a rudder drag correction coefficient, a_H is a coefficient to account for the interaction between the hull and rudder, x_H is the x-coordinate of the point of application of the lift from the hull with respect to amidships, x_R is the x-coordinate of the centre of pressure of the rudder with respect to amidships. δ_R is the rudder's angle. Coefficients a_H and x_H are affected by water depth and are accounted for as discussed in Section 2.3.6.

The rudder's normal force is considerably influenced by the nature of the propeller's slip stream, that is, its wake contraction and velocity. The scheme described by Lee et al. (2003) is used to calculate the effective rudder inflow velocity.

The electromotive oil pressure steering gear model of Son (1989) is used to account for the time lag between the order given for the rudder to be put over, and the machinery's response.

2.3.4. Engine & Propeller Dynamics

The main propulsion engine is based on a four-stroke Diesel cycle burning LNG fuel.

The difference between the resisting torque of the water on the propeller, and the output torque from the engine, results in the acceleration of the drive chain.

Further details of the engine dynamics can be found in Section 2.4.

2.3.5. Propeller

Expressions for the thrust and torque coefficients, K_T and K_Q respectively on a B-Screw Series propeller are obtained from the methods described in Oosterveld and van Oossanen (1975). The calculation scheme for the longitudinal force, X_P, transverse force, Y_P and yawing moment, N_P follows that of equation 4.

$$X_P = (1 - tdf) \rho n^2 D^4 K_T \tag{4a}$$

$$Y_P \approx 0 \tag{4b}$$

$$N_P \approx 0 \tag{4c}$$

Where ρ is water density, n is propeller rotational speed and D is propeller diameter.

The wake fraction at the propeller plane for a ship at zero drift angle, w_{P0} and thrust deduction factor, tdf are calculated from the analysis carried out by Holtrop (1984).

Equation 5, from the work of Hirano (1981), is used to estimate the wake fraction at the propeller plane:

$$w_P = w_{P0} \exp\left(-4.0 \beta_P^2\right) \tag{5}$$

Where the drift angle at the propeller, β_P is given by equation 6

$$\beta_P = \arcsin\left(\frac{v + x_P r}{V_v}\right) \tag{6}$$

x_P is the x-coordinate of the propeller with respect to amidships (a negative value $\approx -0.5 L_{pp}$), v is the sway velocity and V_v is the resultant ship speed.

In this study, the effective wake fraction at zero drift angle w_{P0}, is assumed to be a function of the thrust identity (and hence advance coefficient), following the method of Holtrop (1984).

Throughout this analysis, the ship is operating within the first quadrant, that is, an ahead rotational speed, and ahead speed of advance. A method to correct for the thrust deduction fraction in different quadrants can be found in Harvald (1967). For container ships in shallow water the method proposed by Delefortrie and Vantorre (2007) may be used.

2.3.6. Considerations for the Influence of Confined Water

Shallow water may be defined as $1.2 < h/T < 1.5$ (PIANC, 1992), where h is water depth and T is draught. Shallow water significantly affects ship behaviour (ITTC Manoeuvring Committee, 2002) and is accounted for using the following techniques.

In this study, the hypothesis of Schlighting (1940) is used to estimate speed-resistance relations in shallow water for sub-critical Froude Numbers, with corrections from Lakenby (1963) for blockage effects. Further adaptations from Landweber (1939) are used to account for water of finite width.

The magnitude of the thrust deduction fraction decreases somewhat with decreasing water depth, however, according to Yoshimura (1986) in a practical sense it can assumed to be constant. In the current research this is the assumption made, however there are formulations that account for variation in water depth for particular ships, eg Delefortrie and Vantorre (2007). The wake factor, which increases significantly with decreasing water depth, is corrected for shallow water effects

following the method of Yasukawa (1998). Following the work of NORDCO Ltd. (1989), the variation of roll added mass, and added mass moment of inertia of the propeller with water depth are assumed to be negligible.

Linear manœuvring derivatives are corrected following the method of Kijima (1991). Non-linear manœuvring derivatives are corrected for water depth following methods proposed by Hirano (1985) and Kijima (1989).

Added inertia coefficients are corrected for shallow water following the method of Li and Wu (1990).

Stern flow separation increases with decreasing water depth and thus decreases the effect of the rudder. On the other hand, this is somewhat counterbalanced by the increase in propeller race due to shallow water. In this study, the effect of shallow water on rudder forces has been neglected, however, hull-rudder interaction coefficients are obtained from Kijima et al. (1990), with corrections for shallow water by Yumuro (1985).

Sinkage due to shallow water has been estimated from Tuck and Taylor (1970). Stern trim from the effects of shallow water is estimated from the work of Yoshimura (1986)

The width of the Rhine-Danube-Main canal is used throughout this analysis, namely, 55m width. The depth of the canal is 4m, however a depth of 5.1 metres is used, as the limits of coefficients used for sway and yaw added mass break down at a depth/draught ratio of less than 1.2 (Sheng, 1981). In fact the canal is trapezoidal in cross section, however this is not accounted for in this study.

Whilst the effects of water depth is important on inland waterways, this study concentrates on differences in emissions between steady-state emission factor approaches and estimates accounting for the transient nature of loading variation. Thus, it is not considered of paramount importance at this stage to reproduce to a very high degree of accuracy the effects of shallow water on manœuvring, and indeed, to achieve such accuracy would ideally involve model testing (Vantorre, 2003), beyond the scope of the current study. However, results published by ITTC (2002) indicate encouraging results for the Esso Osaka (Figure 5). The Esso Osaka is one of the few full scale ships for which for which shallow water manœuvring analysis exist (Crane, 1979).

2.4. Numerical Engine Model

Rather than reproducing with a high degree of fidelity the dynamics of a particular physical engine, the developed model is representative of the Diesel cycle, and is used as a basis to provide the thermodynamics, kinetics and transport solver the necessary input parameters.

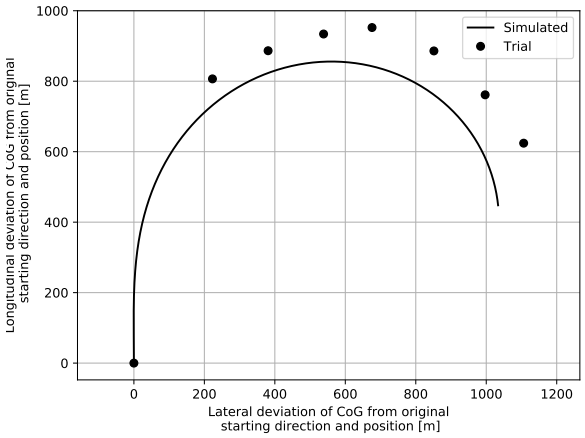

Figure 5: Comparison between results of simulation and trial of a 35° turning circle at a depth/draft ratio of 1.5 of the Esso Osaka at an approach speed of 7 knots.

An example indicator diagram output of the simulated cycle is given in Figure 6. In the process of estimating NO_X formation the numerical model is suitable for a qualitative study of comparing differences in emissions between steady-state design point performance, and transient behaviour.

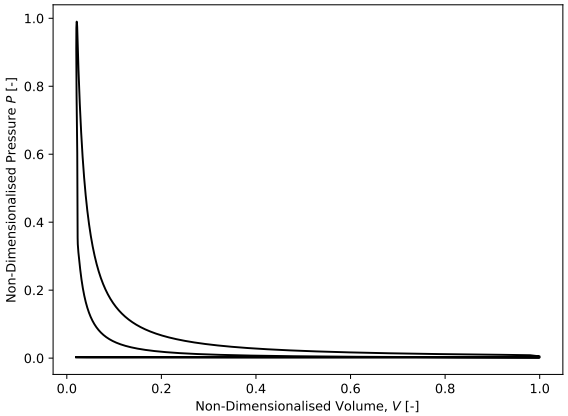

Figure 6: Indicator diagram from engine model.

The instantaneous volume within the cylinder is calculated knowing the cylinder dimensions and instantaneous piston speed. The corresponding pressure and temperature are estimated using *Cantera* (Goodwin et al., 2017), the solver chosen to analyse the thermodynamics, kinetics and transport solutions throughout the simulation.

Essentially, *Cantera* evaluates chemical sources and their properties from established reaction mechanisms,

so as to satisfy the transport processes described by the continuum mechanics and the governing equations for mass, momentum, and energy conservation. The solving of these equations allows the temporal integration of the kinetic system. Cantera handles this efficiently through the use of dedicated nonlinear, differential/algebraic equation solvers (Hindmarsh et al., 2005).

The reaction mechanism used to model the LNG combustion is GRI-Mech 3.0 (Smith et al., 2000). This is a compilation of 325 elementary chemical reactions and associated rate coefficient expressions and thermochemical parameters for the 53 species involved in them. The thermochemistry is based upon standard databases such as those from McBride et al. (1993), and Kee et al. (1990) and contain polynomial fits to specific heats, standard state enthalpies and entropies. It is a proven mechanism and efficient for simulations.

To calculate the thermodynamics, kinetics and transport properties of the combustion process within *Cantera*, the `solution` class is loaded with the reaction mechanisms.

The reactor mechanism used for containing and controlling the chemical reactions within the cylinders is a zero-dimensional model for ideal gas mixtures.

Inlets are defined as a constant-state reservoir, accounting for turbocharger temperature and pressure. The outlet is a constant-state reservoir with ambient temperature, pressure and gas composition properties.

Inlet and outlet reservoirs are connected via the `valve class`, whose mass flow rate is a function of the pressure drop across it, as in equation 7:

$$\dot{m} = K_v \left(P_1 - P_2\right) \tag{7}$$

Where P_1 and P_2 is the pressure of reservoir and reactor respectively. By choosing a suitably large value of K_v, very small pressure differences will result in flow between the reactor mechanism, counteracting any pressure difference.

The injector is modelled via the `MassFlowController class`, maintaining a specified mass flow rate independent of upstream and downstream reactor conditions, and loaded with appropriate values for P, T and fuel composition.

The piston is modelled from the dynamics of a general crank-slider mechanism, as a moving `wall object` separating the reactor (cylinder) from the reservoirs (valves). The piston velocity is defined by Equation 8:

$$v_0\left(t\right) = r_c\ 2\pi n_c\ sin\phi\left(t\right) \tag{8}$$

Where r_c is the crank radius (half the stroke), n_c is the rotational velocity of the crankshaft and ϕ is the crank angle.

The heat flux through the piston wall is computed from:

$$q = U\left(T_{\text{inside}} T_{\text{outside}}\right) + \epsilon\left(T^4_{\text{inside}} - T^4_{\text{outside}}\right) \tag{9}$$

Where U is the overall heat transfer coefficient for conduction/convection, and ϵ is the emissivity. T_{inside} and T_{outside} is the instantaneous temperature inside and outside the cylinder respectively.

The simulation is begun by setting initial conditions for inlet temperature, pressure, gas composition and outlet pressure. At the appropriate crank angle of the engine cycle, using pre-set valve timings, the relationship between mass flow rate and the pressure drop across the valves are set using a constant of proportionality $[kg/s/Pa]$ relationship. This also applies to injection timings where the mass flow rate $[kg/s]$ through the controller is set to a constant value, rather than a function of time, as this level of fidelity is considered excessive at this stage of development.

A `ReactorNet` class is created containing the cylinder, and the `advance` function is used to simultaneously advance the state of the reactor in time (ie solve the governing equations).

2.5. Prediction of NO_X

The `Kinetics class` of *Cantera* is used to evaluate the reaction rates and species production rates within the cylinder (reactor).

Figure 7 shows gas composition results from the simulation and illustrates how, for a particular engine speed, engine operating conditions play a crucial role in NO_X formation when compared with CO_2. This demonstrates the non-linear process of NO_X formation throughout the cycle, in particular during ignition. This phenomenon is not taken into account in the steady-state emission factor approaches, commonly used to assess NO_X emissions.

2.6. Emission Factor Development and Usage

A popular way of estimating emissions is from the use of emission factors, most of which are directly related to fuel consumption, such as those specified in the IMO's Third Greenhouse Gas Study (MEPC, 2014).

For the marine industry, most of these emission factors are based upon generic diesel engines burning medium or heavy fuel oil. In order to illustrate the difference in magnitude of NO_X emissions from steady state and transient operation, an emission factor is developed in this study using the developed simulator.

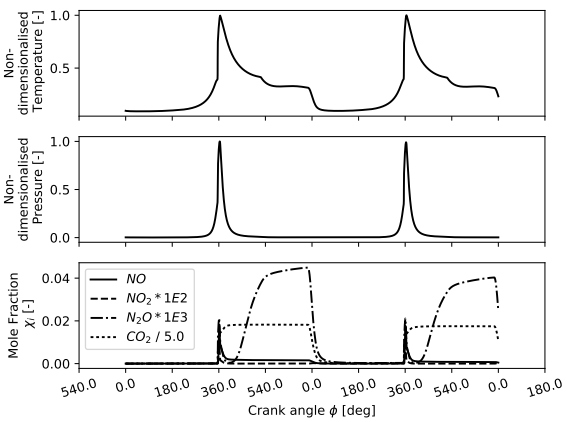

Figure 7: Effects of cylinder operating conditions on NO and CO_2 formation as estimated from simulation.

The resulting emission factor is solely based upon the fuel oil consumption of the engine running at the designed operating conditions.

The emissions estimates which are generated from the use of emission factors are calculated by multiplying the emission factor by the fuel consumption for the particular time step during the simulation.

A reason for calculating an emission factor from the simulation, rather than using one from the literature, is that it is then possible to compare the performance of the same (numerical) engine model which exhibits identical characteristics over a wide range of loading conditions. Without an extremely elaborate engine model, it would be challenging to reproduce an exact model which describes the unsteady response of an existing physical engine which is suitable for unsteady NO_X evaluation. At this stage of the investigation, in which an estimate of the differences in emissions between commonly used steady-state emission factor approaches, and unsteady transient analysis, such an engine model is deemed unnecessary.

2.7. Engine Model Validation

It is challenging to obtain information about the NO_X emissions from an LNG fuelled engine in transient operation that relate in sufficient detail the rate of change of loading, and the subsequent effect on emission formation.

In order to obtain some degree of confidence in the developed numerical model, a 'test' engine is implemented to determine its correlation with established emission factor results. Work conducted by Stenersen and Thonstad (2017) compared on-board measurements of NO_X emissions from ships, and found the average NO_X emissions for LNG fuelled 4-stroke compression ignition engines to be $10.1 g/kg$fuel (or $1.8 g/kWh$), based upon 39 measurements. As part of their study a Wärtsilä 20DF four-stroke engine was used in their analysis of emissions. It is the main dimensions of this engine that is used as a validation test engine in the current study. The main particulars of the engine are listed in Table 2.

Table 2: Particulars of Wärtsilä 20DF test engine.

Cylinder bore	200 mm
Piston stroke	280 mm
Cylinder output	160 kW/cyl
Speed	1000 rpm
Mean effective pressure	22.0 bar

With some manipulation of parameters such as valve timings and inlet temperature and pressures, the numerical model with the main dimensions of the Wärtsilä 20DF was able to produce an output of 152 kW/cyl at a mean effective pressure of 24 bar. The corresponding NO_X emissions were $8.61 g/kg$. This value is considered accurate enough to be useful, especially considering the spread in results from Stenersen and Thonstad (2017).

The authors stress that the results from this analysis may not be indicative of this actual engine's emissions, as there are numerous factors such as piston geometry that are not accounted for in this analysis, which do have an effect on emission production.

3. Results and Discussion of Ship Manœuvring Operation on Exhaust Gas Emissions

For the simulations of the confined water turning circle, and zig-zag manœuvres outlined in Section 2.2, Figures 8 and 9 show a graphical representation of how the percentage differences between the unsteady chemical kinetics based estimates, and the steady-state emission factor based approach vary with time.

Figures 10 and 11 show results for maximum and mean percentage differences for NO_X and CO_2 emissions for the confined water turning circle and zig-zag manœuvres respectively, as described in Section 2.2.

As expected, the CO_2 discrepancy between the two methods is low, indicating that CO_2 can be adequately modelled based upon stoichiometric combustion.

Referring to Figures 10 and 11, as an example, the value of NO_2 formation calculated using the method illustrated in this research for the transient operation is nearly four times that of the steady-state estimate.

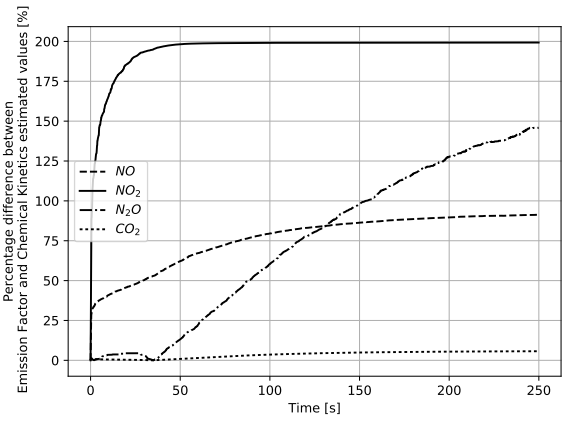

Figure 8: % difference in NO_X emissions between simulated and emission factor prediction with time during turning circle manœuvre in confined water.

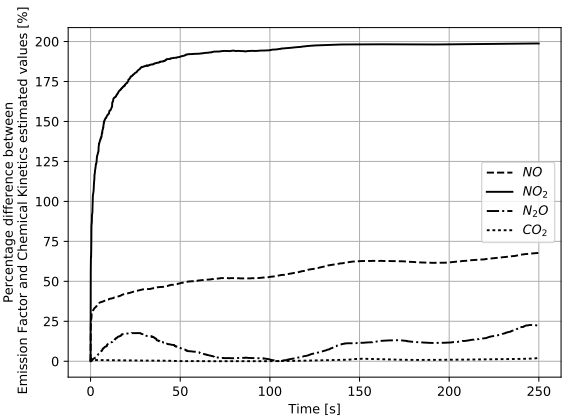

Figure 9: % difference in NO_X emissions between simulated and emission factor prediction with time during 20/20 zig-zag manœuvre in confined water.

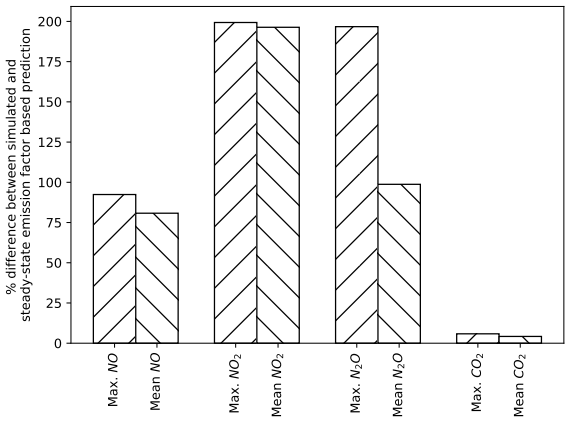

Figure 10: % difference in emissions between simulated and emission factor prediction during turning circle in confined water.

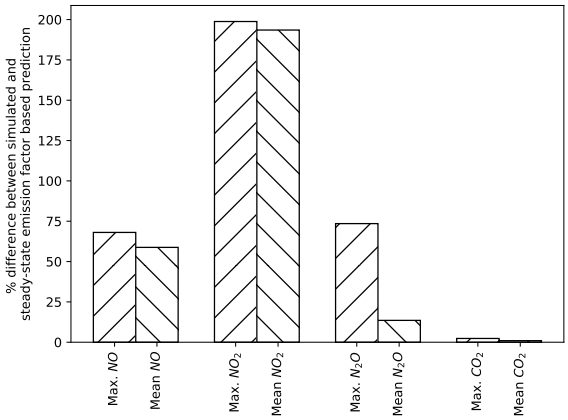

Figure 11: % difference in emissions between simulated and emission factor prediction during zig-zag in confined water.

The interrelated properties of the combustion process and transient engine loading from ship manœuvres indicates that a time-domain simulation lends itself especially well to prediction of NO_X emissions. When used in conjunction with a chemical kinetics solver, this method can provide increased realism and accuracy in the prediction of exhaust gas emissions compared to commonly used steady-state, operation-independent emission factor approaches, whose only dependency is fuel consumption.

An emission factor based upon speed and power could potentially be developed using the proposed method. This emission factor can subsequently be utilised in fast, efficient simulations in a manner suitable for multiple runs. For example in scenarios for conducting emission compliance over different speeds or routes. This can be used to bring awareness to operators regarding NO_X production when used on bridge simulators, akin to a speed-over-ground indicator.

The magnitude in the difference of NO_X formation between steady-state estimates and analysis of transient operation suggests that it would be prudent for future regulations to account for transient operation, especially in areas where a significant amount of manœuvring occurs.

When comparing the differences between the commonly used emission factor approach, and the transient analysis for the turning circle and zig-zag manœuvres, it can be seen that the magnitude of N_2O is markedly different. This indicates that N_2O is more susceptible to transient operation compared to NO and NO_2, and

reflects the generally higher residence time associated with the turning circle manœuvre.

To proceed along these lines of analysis, it is suggested that the development of the engine model is refined to reflect a higher degree of fidelity. The current engine model serves to illustrate the magnitude in differences of NO_X formation between steady-state and transient operation.

4. Conclusions

NO_X production is predominantly a function of engine speed (or residence time) and loading. A time-domain based manœuvring simulator, coupled with an engine model and chemical kinetics solver offers a well suited solution for estimation of NO_X formation.

A manœuvring simulator is used to produce the unsteady loading on the propeller and engine.

It is demonstrated that, due to the attitude of a ship travelling through the water, differences in predicted required power arise compared to that of the steady-state, dead-ahead calm water estimate. It is the latter case that is often used when predicting exhaust gas emission estimates.

It is shown that manœuvring motion has a significant effect on NO_X formation estimates, which are substantially different to the common practice based on the steady-state design point.

During a simulation in confined water to manœuvre the basis vessel over a turning circle described in Section 2.2, the mean difference between steady-state, and transient estimates for NO, NO_2 and N_2O are 76.5%, 195.1%, 74.4% respectively. During the zig-zag manœuvre, the mean differences NO, NO_2 and N_2O are 55.7%, 191.5%, 10.0% respectively. Caution should therefore be employed if using steady-state emission factors when estimating NO_X emissions, especially in areas where manœuvring occurs frequently.

The difference in CO_2 formation is found to be 3.6%, and 0.69% for the confined water turning circle and zig-zag manœuvres respectively, indicating that Stoichiometric combustion based approaches are able to adequately predict CO_2 formation.

It is shown that N_2O is more susceptible to transient loading compared with NO and NO_2.

The presented methodology allows scenarios to be conducted, highlighting areas of a shipping route that are in danger of exceeding permitted limits, or providing solutions for operating strategies to comply with emission regulations.

References

Abkowitz, M. A., 1964. Lectures on ship hydrodynamics - steering and maneuverability. Tech. Rep. HY-5, Hydro and Aerodynamic's Laboratory. Lyngby, Denmark.

Burel, F., Taccani, R., Zuliani, N., 2013. Improving sustainability of maritime transport through utilization of liquefied natural gas (lng) for propulsion. Energy 57, 412 – 420.

Crane, L. C., 1979. Maneuvering trials of a 278 000-dwt tanker in shallow and deep waters. Transactions of SNAME 87, 251 – 283.

Damian, V., Sandu, A., Damian, M., Potra, F. A., Carmichael, G. R., 2017. Kinetic preprocessor. http://people.cs.vt.edu/asandu/Software/Kpp/, last accessed 22nd September 2017.

Delefortrie, G., Vantorre, M., 2007. Modeling the maneuvering behavior of container carriers in shallow water. Journal of Ship Research 51 (4), 287–296.

Delefortrie, G., Vantorre, M., Eloot, K., 2005. Modelling navigation in muddy areas through captive model tests. Journal of marine science and technology 10 (4), 188–202.

Eloot, K., Vantorre, M., 2003. Development of a tabular manoeuvring model for hull forces applied to full and slender ships in shallow water. In: International Conference on Marine Simulation and Ship Maneuverability, MARSIM. Vol. 3. pp. 25–28.

Goodwin, D. G., Moffat, H. K., Speth, R. L., 2017. Cantera: An object-oriented software toolkit for chemical kinetics, thermodynamics, and transport processes. `http://www.cantera.org`, version 2.3.0.

Harvald, S., 1967. Wake and thrust deduction at extreme propeller loadings. Tech. rep., Publications of the Swedish State Shipbuilding Experimental Tank, Nr. 61.

Hindmarsh, A. C., Brown, P. N., Grant, K. E., Lee, S. L., Serban, R., Shumaker, D. E., Woodward, C. S., 2005. Sundials: Suite of nonlinear and differential/algebraic equation solvers. ACM Transactions on Mathematical Software (TOMS) 31 (3), 363–396.

Hirano, M., 1981. A practical calculation method of ship maneuvring motion at initial design stage. Naval Architecture and Ocean Engineering. 19.

Hirano, M., 1985. Estimation of maneuvrabilities of a ship in shallow water. Society of Naval Architects of Japan Bulletin 668.

Holtrop, J., 1984. A statistical re-analysis of resistance and propulsion data. International Shipbuilding Progress., 272 – 276.

Hountalas, D. T., 2000. Prediction of marine diesel engine performance under fault conditions. Appl. Therm. Eng., 1753 – 1783.

IMO, 2005. Marpol 73/78 annex vi.regulations for the prevention of air pollution from ships. Tech. rep., International Maritime Organisation.

Inoue, S., Hirano, M., Kijima, K., Takashina, J., 1981. A practical calculation method of ship manoeuvring motion. International Shipbuilding Progress. 28.

ITTC, 2002. The specialist committee on esso osaka - final report and recommendations to the 23rd ittc. In: 23rd ITTC. International Towing Tank Conference.

ITTC Manoeuvring Committee, 2002. Final report and recommendations to the 23rd ittc. In: Proc. of the 23rd International Towing Tank Conference, Venice, Italy.

Kampa, M., Castanas, E., 2008. Human health effects of air pollution. Environmental Pollution 151 (2), 362 – 367, proceedings of the 4th International Workshop on Biomonitoring of Atmospheric Pollution (With Emphasis on Trace Elements).

Kee, R., Rupley, F., Miller, J., 1990. The chemkin thermodynamic data base. Tech. Rep. SAND87-8215B, Sandia National Laboratories.

Kijima, K., 1989. Mss report ii: Mathematical model for the manoeu-

vring motions of a ship in shallow water. Society of Naval Architects of Japan Bulletin 718.

Kijima, K., 1991. Prediction method for ship manoeuvring performance in deep and shallow waters. Workshop on modular manoeuvring models, The Society of Naval Architects and Marine Engineers.

Kijima, K., Katsuno, T., Nakiri, Y., Furakawa, Y., 1990. On the manoeuvring performance of a ship with the parameter of loading condition. Society of Naval Architects of Japan 168.

Kilpinen, P., 2010. Optimization of a simplified sub-model for no emission prediction by cfd in large 4-stroke marine diesel engines. Fuel Process. Technol., 218 – 228.

Kongsberg Gruppen, 2017. Kongsberg maritime simulation and training ship's bridge simulator.

Lakenby, H., 1963. The effect of shallow water on ship speed. Shipbuilder and Marine Engine Builder 70.

Landweber, L., 1939. Tests on a model in restricted channels. Tech. Rep. EMB 460, David Taylor Research Center.

Lee, T., Ahn, K., Lee, H., Yum, D., 2003. On an empirical prediction of hydrodynamic coefficients for modern ship hulls. In: MARSIM '03. Hyundai Heavy Industries Co., Ltd, Korea.

Li, M., Wu, X., 1990. Simulation calculation and comprehensive assessment on ship maneuverabilities in wind, wave, current and shallow water. In: Proceedings of the Joint International Conference on Marine Simulation (MARSIM 90) and Ship Maneuverability (ICSM '90). pp. 403–411, 459–465.

McBride, B. J., Gordon, S., Reno, M. A., 1993. Coefficients for calculating thermodynamic and transport properties of individual species. Tech. Rep. TM-4513, NASA.

MEPC, 2014. Reduction of GHG emissions from ships, Third IMO GHG study 2014 final report. Tech. Rep. MEPC 67/INF.3, Marine Environment Protection Committee, London, UK.

Murphy, A., Norman, A., Pazouki, K., Trodden, D., 2015. Thermodynamic simulation for the investigation of marine diesel engines. Ocean Engineering 102, 117 – 128.

Murphy, A., Pazouki, K., 2012. Exhaust gas emissions from regional shipping: Mitigating technologies and emission prediction. In: International conference on The Environmentally Friendly Ship, London: The Royal Institution of Naval Architects.

NORDCO Ltd., 1989. Development of mathematical model to predict ship maneuvering, part i: Formulations and verifications. Tech. rep., National Recearch Council (Canada).

Oltmann, P., Sharma, S., 1984. Simulation of combined engine and rudder maneuvers using an improved model of hull-propeller-rudder interactions. Tech. Rep. 444, Technische Universität Hamburg-Harburg, Hamburg, prepared for the Fifteenth ONR Symposium on Naval Hydrodynamics.

Oosterveld, M., van Oossanen, P., 1975. Further computer-analysed data of the wageningen b-screw series. International Shipbuilding Progress. 22.

PIANC, 1992. Capability of ship manoeuvring simulation models for approach channels and fairways in harbours. Supplement to PIANC Bulletin No. 77 Report of Working Group no. 20 of Permanent Technical Committee II, The World Association for Waterborne Transport Infrastructure.

Reaction Design, 2017. Chemkin. http://www.reactiondesign.com/products/chemkin/chemkin-2/, last accessed 22nd September 2017.

Schlighting, O., 1940. Ship resistance in water of limited depth. Tech. rep., U.S. Experimental Model Basin, Navy Yard, Washington, D.C.

Seitz, M., Karpatyova, L., van Dooren, N., Janssen, A., 2015. Lng masterplan for rhine/meuse-main-danube. Tech. Rep. 2012-EU-18067-S, Pro Danube Management GmbH (Austria) and Port of Rotterdam Authority.

Sheng, Z. Y., 1981. Discussion of manoeuvrability committee report. In: 16th ITTC Manoeuvring Committee Report.

Smith, G. P., Golden, D. M., Frenklach, M., Moriarty, N. W., Eiteneer, B., Goldenberg, M., Bowman, C. T., Hanson, R. K., Song, S., William C. Gardiner, J., Lissianski, V. V., Qin, Z., 2000. An optimized mechanism designed to model natural gas combustion. `http://www.me.berkeley.edu/gri_mech/`.

Soares, C. G., Dejhalla, R., Pavletic, D. (Eds.), 2015. Towards Green Marine Technology and Transport. CRC Press, Taylor & Francis Group, London, from section 'Numerical simulation of a two-stroke marine diesel engine' by M. Tadros, M. Ventura and C. Guedes Soares.

Son, K., 1989. On the mathematical model for estimating the manoeuvring performance of ships. Society of Korea Voyage. 13 (2).

Stenersen, D., Thonstad, O., 2017. Ghg and nox emissions from gas fuelled engines. Tech. Rep. OC2017 F-108, SINTEF.

Trodden, D., Woodward, M., Atlar, M., 2016. Accounting for ship manoeuvring motion during propeller selection to reduce co2 emissions. Ocean Engineering 123, 346 – 356.

Tuck, E., Taylor, P., 1970. Shallow water problems in ship hydrodynamics. In: 8th, Symposium Naval Hydrodynamics. Office of Naval Research.

Vantorre, M., 2003. Review of practical methods for assessing shallow and restricted water effects. In: International Conference on Marine Simulation and Ship Maneuverability (MARSIM'03).

Yasukawa, H., 1998. Computation of effective rudder forces of a ship in shallow water. In: Proceedings, Symposium of Forces Acting on a Manoeuvring Vessel (MAN98). pp. 125–133.

Yoshimura, Y., 1986. Mathematical model for the manoeuvring ship motion in shallow water. Kansai Society of Naval Architects 200, 41 – 51.

Yumuro, A., 1985. Some experiments on shallow water effects on maneuvring hydrodynamic forces acting on a ship model. IHI Engineering Review 25 (4).

Zeldovich, Y. B., 1946. The oxidation of nitrogen in combustion and explosions. Acta Physiochimica U.R.S.S., XXI, Academy of Science of the USSR, 577 – 628.